

Full Length Article

Reduced magnetic coercivity and switching field in NiFeCuMo/Ru/NiFeCuMo synthetic-ferrimagnetic nanodots



X. Li^a, C.W. Leung^b, C.-C. Chiu^c, K.-W. Lin^c, Mansun Chan^d, Y. Zhou^e, Philip W.T. Pong^{a,*}

^a Department of Electrical and Electronic Engineering, The University of Hong Kong, Hong Kong

^b Department of Applied Physics, The Hong Kong Polytechnic University, Hong Kong

^c Department of Materials Science and Engineering, National Chung Hsing University, Taichung 402, Taiwan

^d Department of Electronic and Computer Engineering, Hong Kong University of Science and Technology, Hong Kong

^e School of Science and Engineering, The Chinese University of Hong Kong, Shenzhen, 518172, China

ARTICLE INFO

Article history:

Received 30 December 2016

Received in revised form 2 March 2017

Accepted 9 March 2017

Available online 11 March 2017

Keywords:

Synthetic-ferrimagnetic

Nanodots

Nanosphere lithography

ABSTRACT

The coercivity (H_c) and switching field (H_{sw}) of free layers increase remarkably with shrinking structural dimensions, reducing the sensitivity of nanosized magnetoresistive sensors. In this work, conetic-alloy (NiFeCuMo) synthetic ferrimagnetic (SyF) trilayers are proposed to reduce H_c and H_{sw} in magnetic nanostructures. SyF stacks of NiFeCuMo/Ru/NiFeCuMo were patterned into nanodot arrays with diameter of 60 nm by nanosphere lithography. The thickness of Ru layer was chosen so that high interlayer coupling energy existed in the continuous film. The linear dependence of H_c and H_{sw} of SyF nanodot on the amplification factor was revealed. Magnetic field annealing was conducted at various temperatures (T_{an}) ranging from 373 K to 673 K. Annealing at low temperature ($T_{an} \leq 473$ K) relaxed the structural disorders, resulting in reduced surface roughness and decreased H_c and H_{sw} . Higher T_{an} changed the preferred orientations in the crystalline structures, leading to increased roughness and higher H_c and H_{sw} . This work shows that the H_c and H_{sw} of nanostructures can be reduced through engaging Conetic alloy in SyF stack. The Conetic-alloy-based SyF structures are a promising candidate as free layers in nanosized spintronic devices.

© 2017 Elsevier B.V. All rights reserved.

1. Introduction

The broad application of nanometric spintronic devices is facilitated by the development of high-quality spin valves. In these devices, ferromagnetic (FM) materials with small switching field (H_{sw}) are required as free layers to enable sensitive response to external excitations such as magnetic field or spin-transfer torque. Besides, low coercivity (H_c) are also preferred to reduce the hysteresis effect. However, the H_c and H_{sw} of nanostructures are typically much larger than that in the planar films due to the increased influence of demagnetization field at the structural edges [1]. Although H_c and H_{sw} can be reduced through decreasing the layer thickness, a drawback of increased thermal fluctuation is incurred, especially when the thin film is patterned into nanoscale [2]. The synthetic ferrimagnetic (SyF) structure is a trilayer stack containing two FM layers sandwiching a thin nonmagnetic layer. The two FM layers couple antiferromagnetically (AF) through Ruderman-Kittel-

Kasuya-Yosida (RKKY) interaction, resulting in reduced effective thickness while maintaining high thermal stability [3]. The introduction of SyF as free layers have brought various benefits in spintronic devices such as high sensitivity in nanometric magnetoresistive (MR) sensors [4], high quality factor in spin-torque oscillators (STO) [5], and low critical current in magnetic random access memories (MRAM) [6].

Soft magnetic materials such as NiFe or CoFeB were conventionally used in spin valves due to the low H_c ($\mu_0 H_c \sim 0.4$ mT) and small H_{sw} ($\mu_0 H_{sw} \sim 1.5$ mT) in continuous films [7]. Conetic alloy (Ni₇₇Fe₁₄Cu₅Mo₄) is an FM material with smaller H_c than traditional soft magnetic materials such as CoFeB and NiFe [8–10]. By using Conetic alloy as free layer in micrometer-sized MR sensors, sensitivity of 3%/mT and $\mu_0 H_c$ smaller than 0.1 mT was achieved in the low field regime [11,12], which enabled the detection of weak magnetism such as iron-oxide nanoparticles [13]. Recently, low $\mu_0 H_c$ of 0.03 mT was reported in spin valve sheet films with Conetic-alloy-based SyF free layer [14], revealing the great promise of Conetic alloy. While the previous reports on SyF stacks based on NiFe [3], CoFe [15], NiFeCo [16] and CoFeB [17,18] have shown reduced H_c and H_{sw} compared with single layers, the mag-

* Corresponding author.

E-mail address: ppong@eee.hku.hk (P.W.T. Pong).

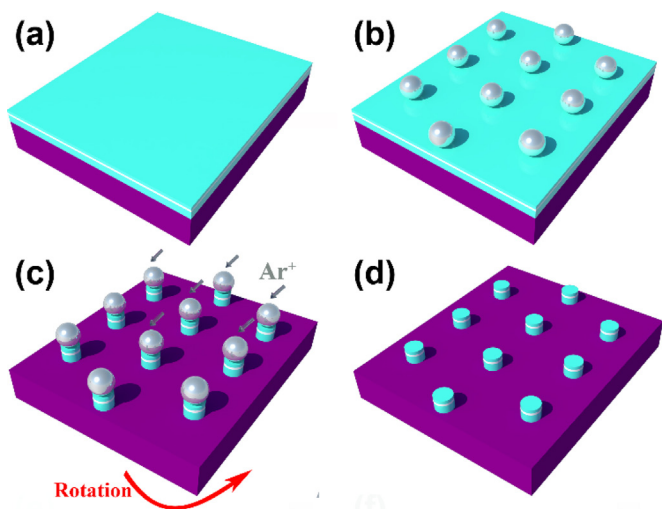


Fig. 1. Fabrication process of nanodot arrays: (a) thin-film stack sputtering, (b) nanosphere mask deposition, (c) tilted ion milling with rotation, and (d) removal of residual spheres.

netic properties of Conetic-alloy-based SyF nanostructures remain unclear. Meanwhile, annealing was reported to be beneficial for reducing H_c of the MR sensor with Conetic alloy free layer [11]. An experimental investigation on the magnetic properties and annealing effect of Conetic-alloy-based SyF nanodots will be beneficial for developing soft free-layer materials for nanometric spintronic devices. Besides, nanosphere lithography [19] is a cost-effective nanofabrication technique that is capable of parallel production of nanostructures on a large area. Its high yield for nanostructure fabrication made it a suitable method for this research.

In this work, the thickness of Ru in NiFeCuMo/Ru/NiFeCuMo SyF continuous films was firstly optimized to guarantee strong RKKY coupling. The magnetic properties of SyF nanodots with different NiFeCuMo layer thicknesses were then comparatively studied with that of the single-layer nanodots. Finally, magnetic field annealing was conducted on the SyF films and nanodots to explore the influence of annealing temperature (T_{an}) on the microstructures and magnetic properties.

2. Material and methods

The samples under investigation were multilayers of Si/SiO₂/Ta 3.5/Cu 5/Ni₇₇Fe₁₄Cu₅Mo₄ t_F /Ru t_{Ru} /Ni₇₇Fe₁₄Cu₅Mo₄ 3/Ta 3.5 (thickness in nanometers). The sputtering rate of NiFeCuMo and Ru was 0.44 nm/min and 0.56 nm/min, respectively. t_{Ru} was varied from 0.5 nm to 1.3 nm by controlling the sputtering time to investigate the thickness dependence of the antiferromagnetic coupling between two Conetic alloy layers. The thickness dependence of H_c and H_{sw} was studied through changing t_F from 5 nm to 11 nm. The fabrication process of the nanodot arrays was similar to that reported in references [20,21]. The multilayers were sputtered on 1 cm × 1 cm Si/SiO₂ substrate under in-plane magnetic field of 30 mT to define the easy axis (Fig. 1(a)). The thin film surface was then treated with positive electrolyte (Poly(diallyldimethylammonium chloride)). Negatively charged 120-nm polystyrene nanospheres were adsorbed on the surface by electrical static adsorption (Fig. 1(b)). The samples were then etched by a KRI KDC-10 ion source for 3 min with sample rotation at 37 rpm. The materials that were not protected by the nanospheres were etched by the tilted (~45°) ion beam, forming non-close-packed dot arrays (Fig. 1(c)). Toluene rinse with sonication was subsequently engaged to remove the residual spheres (Fig. 1(d)).

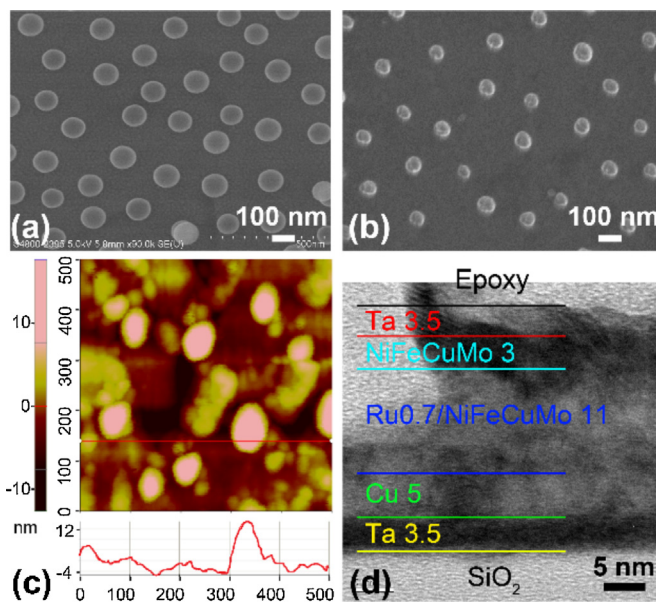


Fig. 2. The planar view of (a) the polystyrene nanospheres and (b) the nanodot arrays obtained by SEM. (c) The AFM image and (d) the cross-sectional TEM image of the nanodot with $t_F = 11$ nm.

The SyF continuous films and nanodots with $t_F = 7$ nm were vacuum annealed at 373 K–673 K for 1 h. During the annealing, the magnetic field of 0.15 T was applied along the easy axis. The easy-axis magnetization hysteresis loops were measured by a Microsense EZ7 vibrating sample magnetometer (VSM) at room temperature. H_{sw} refers to the magnetic field of the coherent switching of the AF-coupled FM layers (i.e. the saturation field of the minor hysteresis loop) [3]. The planar view of the nanosphere masks and nanodot arrays was obtained by a Hitachi S4800 field-emission scanning electron microscope (FE-SEM). The cross-sectional morphologies of the nanodot arrays were observed by a Tecnai G2 high-resolution transmission electron microscope (HRTEM). The surface morphologies of the planar films and nanodots were characterized by a Parker XE-150 atomic force microscope (AFM) operating in tapping mode. The crystalline phase structures of the planar films were characterized by a Bruker AXS D8 Advance grazing incidence (0.5°) X-ray diffraction (GIXRD) spectrometer.

3. Results and discussions

The SEM images of the nanosphere masks and nanodot arrays are shown in Fig. 2(a) and (b), respectively. Non-close-packed spheres are uniformly distributed with average diameter of 120 nm and average center-to-center distance of 220 nm. After the ion milling process, the diameters of the dots were reduced to around 60 nm. This is because the side wall of the nanodots were also etched by the tilted Ar⁺ ion beam. The dot-to-dot interactions are relatively weak due to the large distances amongst the cells. The height of the patterned nanodot is around 17 nm, as measured by AFM (Fig. 2(c)). The multilayer structure in the nanodot is revealed by the cross-sectional TEM image in Fig. 2(d). The 0.7-nm-thick Ru layer is indistinguishable from the adjacent Conetic-alloy layer, due to the restriction in the resolution of the TEM. The ion milling stopped near the interface between the bottom Conetic alloy and Cu seeding layer. This interface is blurred in the TEM image due to the diffusion and intermixing of Cu during the preparation of the TEM sample slice.

The influence of t_{Ru} in SyF continuous films were investigated while t_F was maintained at 7 nm. The easy-axis hysteresis loops

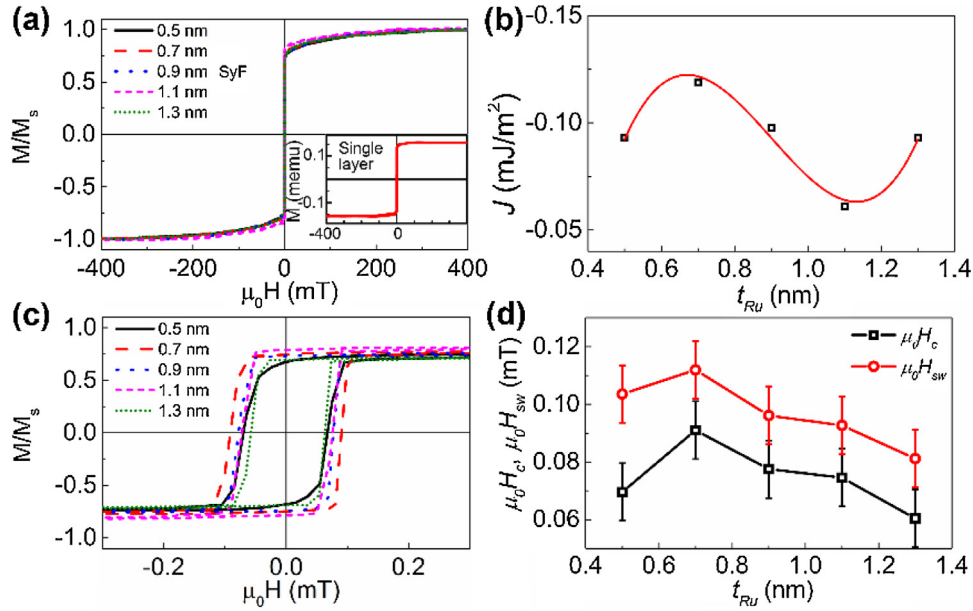


Fig. 3. (a) The normalized full magnetization hysteresis loops of NiFeCuMo 7/Ru t_{Ru} /NiFeCuMo 3 continuous films as t_{Ru} is varied from 0.5 nm to 1.3 nm (inset: the hysteresis loop of 3-nm-thick NiFeCuMo single layer). (b) The coupling energy as a function of t_{Ru} , (c) the minor hysteresis loops, and (d) $\mu_0 H_c$ and $\mu_0 H_{sw}$ as a function of t_{Ru} .

exhibit large saturation field ($\mu_0 H_{sat} \sim 50$ mT–100 mT in Fig. 3(a)), which is much higher than that of the 3-nm-thick Conetic single layer (~ 1.5 mT in the inset of Fig. 3(a)). The higher H_{sat} is attributed to the establishment of AF coupling between the two FM layers. The interlayer coupling energy (J) can be calculated from [22]:

$$J = \mu_0 H_{sat} M_s \frac{t_1 t_2}{t_1 + t_2} \quad (1)$$

where $M_s = 5.3 \times 10^5$ A/m is the saturation magnetization which is acquired from the inset of Fig. 3(a), while t_1 and t_2 are the thickness of the two Conetic-alloy layers respectively. The calculated coupling energy exhibits oscillatory dependence on t_{Ru} (Fig. 3(b)), which is consistent with the previous reports on CoFeB/Ru/CoFeB trilayer [18] and NiFe/Au multilayers [23]. The maximum J of -0.12 mJ/m² was achieved with $t_{Ru} = 0.7$ nm. The smaller J compared with the CoFe-based SyF film (-4.2 mJ/m² as calculated from reference [15]) and the CoFeB-based SyF film (-0.15 mJ/m² in reference [18]) reveals the relatively weak RKKY coupling in Conetic-alloy-based SyF stacks. This is also responsible for the small intermediate plateaus in the hysteresis loops, which correspond to the AF alignment of the two FM layers. The minor hysteresis loops of SyF stack were measured at field step of 0.02 mT and shown in Fig. 3(c). The sharp switching in the minor loops indicates a reversal mechanism of coherent rotation of multi-domains in both FM layers. The coercivity and switching field are plotted as a function of t_{Ru} in Fig. 3(d). H_c reaches maximum when $t_{Ru} = 0.7$ nm. The decreasing H_c at higher t_{Ru} is attributed to the emergence of ferromagnetic coupling between the two FM layers [15]. In the following investigation, $t_{Ru} = 0.7$ nm was used since strong interlayer coupling energy was needed to maintain the AF alignment between the two FM layers. The AF alignment guaranteed small exchange coupling energy and thus small H_c in nanometric elements [15].

The magnetic properties of SyF nanodots ($t_F = 5$ –11 nm) and single-layer nanodots (6 nm in thickness) based on Conetic alloy are compared in Fig. 4. Curved hysteresis loops with low squareness are observed (Fig. 4(a)), and they were due to the increased edge effect in nanostructures [24,25]. The $\mu_0 H_c$ (0.23–1.7 mT) and $\mu_0 H_{sw}$ (1–5.8 mT) of the SyF nanodots were all smaller than the single-layer Conetic alloy nanodot (cf. $\mu_0 H_c = 2.00 \pm 0.01$ mT and $\mu_0 H_{sw} = 7.00 \pm 0.01$ mT). This is because the demagnetization field

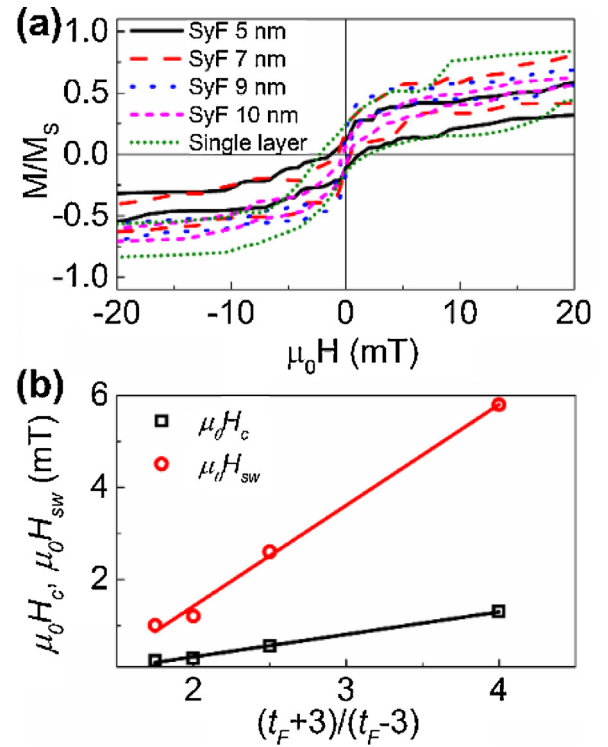


Fig. 4. (a) The minor hysteresis loops of nanodots of SyF stack and single layer at different t_F , and (b) $\mu_0 H_c$ and $\mu_0 H_{sw}$ as a function of the amplification ratio.

at the edges of the nanodots were reduced by the RKKY coupling between the two FM layers [16,26]. When the two FM layers in SyF stack were AF-coupled, H_c of an ideal circular dot can be interpreted from the anisotropy energy [15]:

$$H_c = \frac{2K_u}{M_s} \frac{t_1 + t_2}{t_1 - t_2} \quad (2)$$

where K_u is the uniaxial anisotropy. The term $(t_1 + t_2)/(t_1 - t_2)$ is defined as the amplification factor (α). As shown in Fig. 4 (b), the measured H_c and H_{sw} exhibited similar linear relation with α , which

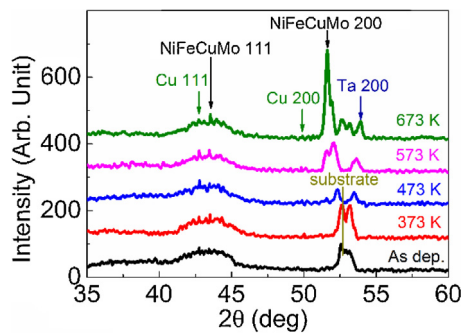


Fig. 5. The GIXRD patterns of the as-deposited and field-annealed SyF continuous films.

is consistent with the theoretical prediction in Eq. (2). Smaller H_c and H_{sw} were achieved when the thickness difference between the two FM layers became larger [16]. The intercept was believed to be resulted from the misaligned spins in the edges of the nanodots. These results show that the Conetic-alloy-based SyF trilayer possessed smaller H_c and H_{sw} than single layers in nanostructures. Better soft magnetic performance can be achieved through tailoring the thickness of both FM layers.

Since magnetic field annealing was widely adopted in the fabrication of spin valves [27], the influence of T_{an} on the microstructures and magnetic properties of SyF ($t_F = 7$ nm) nanodots and continuous films were further investigated. The GIXRD patterns of the as-deposited and field-annealed SyF continuous films are shown in Fig. 5. Diffraction peaks of face-centered cubic (FCC) Cu (111) grains were observed at 42.7° . The Cu seeding layer promoted the formation of NiFeCuMo (111) texture, as evidenced by the diffraction peak at $2\theta = 43.5^\circ$ in all samples. This is consistent with the previous reports on the crystalline structures of NiFeCuMo grown on Ta buffer layer [8]. After annealing at high temperature ($T_{an} > 573$ K), diffraction peaks of Ta (200) (at $2\theta = 54^\circ$), NiFeCuMo (200) (at $2\theta = 51.5^\circ$) and Cu (200) (at $2\theta = 50^\circ$) emerged. The mitigation of Mo and Cu atoms after high-temperature annealing may further enhance the formation of NiFe (200) crystallites. The formation of grains with different orientations indicates that the high-temperature annealing altered the preferred orientation of the crystalline structures from (111) to (200). The diffraction peak at $2\theta = 52.5^\circ$ was believed to be resulted from the Si/SiO₂ substrate [28].

The surface morphologies of the as-deposited and field-annealed SyF continuous films were characterized by AFM and shown in Fig. 6. The as-deposited samples exhibited high root mean square (RMS) roughness of 0.42 nm. The small pits and spikes on the thin film surface were evidence of the defects and grain boundaries in the thin film. During the field annealing, the structural disorders were relaxed and smooth surfaces were formed. The minimum R_q of 0.22 nm was acquired after annealing at 473 K (Fig. 6(d)). As T_{an} further increased, the Conetic alloy were crystallized at (200) orientation, as evidenced by the XRD patterns in Fig. 5. The grain growth after high-temperature annealing [29] resulted in smooth but curved surface (Fig. 6(e)). R_q increased to 0.39 nm when $T_{an} = 673$ K.

The structural modifications induced by the field annealing at various T_{an} resulted in remarkable changes in the magnetic properties. The minor hysteresis loops of the as-deposited and field-annealed continuous films and SyF nanodots are shown in Fig. 7(a) and (b), respectively. The remanence of continuous films decreased dramatically after annealing at 673 K. The low remanence ($M_r/M_s \sim 0.15$) and the high saturation field ($\mu_0 H_{sat} \sim 0.2$ T, higher than the annealing field of 0.15 T) indicate that high-temperature annealing affected the domain structures by creating a distribution of uniaxial anisotropies deflecting away from the easy axis [30]. As a result, the magnetic moment along the easy axis was reduced, and high external field was required to align the disordered spins. On the other hand, the field-annealed nanodot arrays exhibited similar remanence (0.25) with the as-deposited samples. Since the SyF nanodot exhibited single-domain structure due to the RKKY coupling [31], the antiparallel coupling was maintained during high-temperature annealing [18]. The H_c and H_{sw} of nanodots and continuous films presented similar annealing effect (Fig. 4(c)). When $T_{an} \leq 473$ K, H_c and H_{sw} decreased with increasing T_{an} . The reduced H_c is attributed to the enhanced crystalline fitness at interfaces [8], as evidenced by the reduced R_q in Fig. 6. However, further increasing T_{an} to 673 K resulted in remarkable increase in H_c and H_{sw} , especially in the nanodot arrays. This was caused by the crystallization of NiFeCuMo (200) crystallites, similar to the case of CoFeB [18]. The minimum coercivity ($\mu_0 H_c = 0.41 \pm 0.01$ mT) and switching field ($\mu_0 H_{sw} = 1.60 \pm 0.01$ mT) were achieved after annealing at 473 K. This corresponds to a 25.5% decrease in H_c and 38.5% decrease in H_{sw} compared with the as-deposited sample. These results show that the magnetic properties can be further tailored by magnetic field annealing.

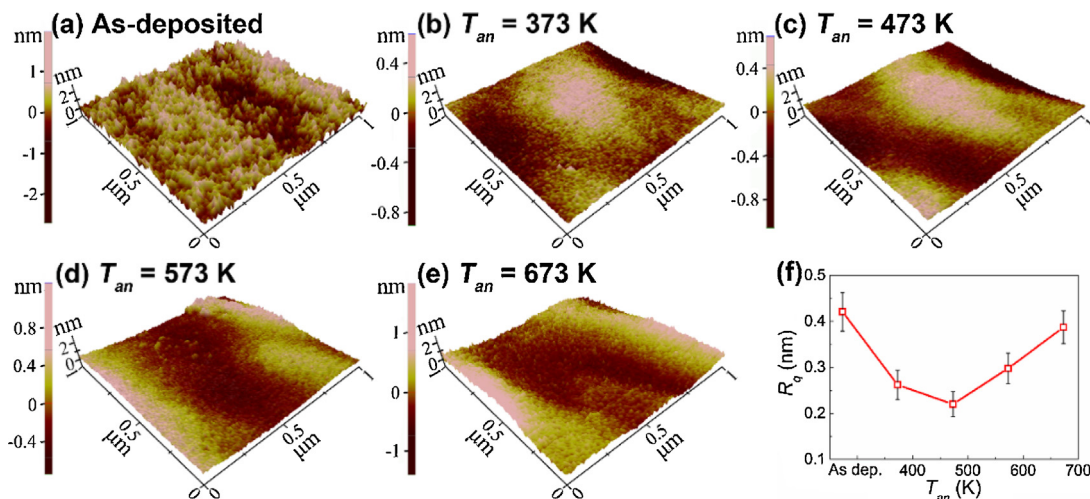


Fig. 6. (a)–(e) The AFM images ($1 \mu\text{m} \times 1 \mu\text{m}$) and (f) RMS roughness measured on as-deposited and field-annealed continuous films (The error bars refer to the standard deviation of R_q measured on three regions).

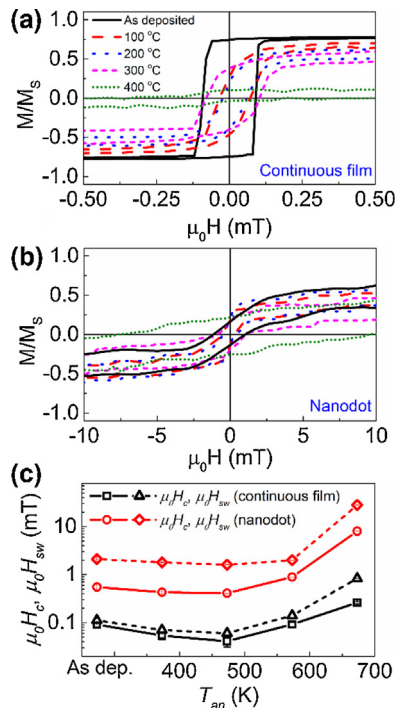


Fig. 7. The minor hysteresis loops of as-deposited and field-annealed (a) continuous films and (b) nanodot arrays of SyF stack, and (c) H_c and H_{sw} as a function of the annealing temperature.

The above results have revealed the low H_c and H_{sw} in the as-deposited ($\mu_0 H_c = 0.23 \pm 0.01$ mT, and $\mu_0 H_{sw} = 1.00 \pm 0.01$ mT when $t_F = 11$ nm) and field-annealed ($\mu_0 H_c = 0.41 \pm 0.01$ mT, and $\mu_0 H_{sw} = 1.60 \pm 0.01$ mT when $t_F = 7$ nm) SyF nanodots based on Conetic alloy. These values are smaller than that of the nanostructures based on Conetic alloy or Supermalloy ($\mu_0 H_c = 24$ mT [32]) single layer, and they are also lower than that of the SyF nanostructures based on other FM materials, such as NiFeCo-based SyF nanodots (cf. $\mu_0 H_{sw} = 2.2$ mT [16]), NiFe-based SyF nanodots (cf. $\mu_0 H_{sw} = 2$ mT [3]), and CoFeB-based SyF nanodots (cf. $\mu_0 H_c = 5$ mT [33]). The Conetic-alloy-based SyF stack can provide small H_c and H_{sw} in the nanometric regime, and its magnetic properties can be further fine-tuned by adjusting the thickness of FM layers and fine tuning the annealing temperature. This type of stack is suitable for applications in nanosized spintronic devices that require soft magnetic free layer.

4. Conclusions

Conetic-alloy-based SyF nanodot arrays were prepared by nanosphere lithography, and the thickness dependence and annealing effect of the microstructures and magnetic properties were investigated. The interlayer coupling energy between the two FM layers exhibited oscillatory dependence on t_{Ru} . The maximum coupling energy occurred at $t_{Ru} = 0.7$ nm, while the smallest H_c and H_{sw} were observed in SyF thin films with $t_{Ru} = 1.3$ nm. The H_c and H_{sw} of SyF nanodots were much smaller than that of the single-layer nanodots, and exhibited linear relation with the amplification factor. Magnetic field annealing at low temperature ($T_{an} \leq 473$ K) resulted in lower surface roughness and reduced H_c and H_{sw} . On the other hand, higher annealing temperature led to the changes in the crystalline orientation from (111) to (200) as well as the increase in surface roughness. These structural changes tended to increase H_c and H_{sw} . The minimum $\mu_0 H_c$ of ~ 0.41 mT and $\mu_0 H_{sw}$ of ~ 1.6 mT was achieved in SyF nanodots after field annealing at 473 K. These results have proved that nanostructures with Conetic-alloy-

based SyF geometry exhibit lower H_c and H_{sw} than nanostructures of Conetic-alloy single layer or SyF multilayer based on conventional soft magnetic materials. This work provides insight into novel multi-layered structures for developing soft magnetic free layers for nanosized spintronic devices such as spintronic sensors.

Acknowledgment

This research is supported by the Seed Funding Program for Basic Research, Seed Funding Program for Applied Research and Small Project Funding Program from the University of Hong Kong, ITF Tier 3 funding (ITS-104/13, ITS-214/14), and University Grants Committee of Hong Kong (AoE/P-04/08). C. W. L. acknowledges the support by The Hong Kong Polytechnic University (G-YM43/G-YB1). Y.Z. acknowledges the support by the National Natural Science Foundation of China (No. 11574137) and the Shenzhen Fundamental Research Fund (No. JCYJ20160331164412545).

References

- [1] A. Ercole, A.O. Adeyeye, C. Daboo, J.A.C. Bland, D.G. Hasko, Finite size effects in the static and dynamic magnetic properties of FeNi wire array structures, *J. Appl. Phys.* 81 (1997) 5452–5454.
- [2] V. Baltz, G. Gaudin, P. Somani, B. Dieny, Influence of edges on the exchange bias properties of ferromagnetic/antiferromagnetic nanodots, *Appl. Phys. Lett.* 96 (2010) 262505.
- [3] Y.M. Lee, Y. Ando, T. Miyazaki, H. Kubota, Reduction of switching fields of submicrometer sized magnetic tunnel junction with NiFe-based synthetic ferrimagnetic free layer, *J. Appl. Phys.* 101 (2007) 023905.
- [4] P. Coelho, D.C. Leitao, J. Antunes, S. Cardoso, P.P. Freitas, Spin Valve Devices With Synthetic-Ferrimagnet Free-Layer Displaying Enhanced Sensitivity for Nanometric Sensors, *IEEE Trans. Magn.* 50 (2014) 1–4.
- [5] T. Nagasawa, K. Kudo, H. Suto, K. Mizushima, R. Sato, Large-amplitude, narrow-linewidth microwave emission in a dual free-layer MgO spin-torque oscillator, *Appl. Phys. Lett.* 105 (2014) 182406.
- [6] J. Hayakawa, S. Ikeda, K. Miura, M. Yamanouchi, L. Young Min, R. Sasaki, M. Ichimura, K. Ito, T. Kawahara, R. Takemura, T. Meguro, F. Matsukura, H. Takahashi, H. Matsuoka, H. Ohno, Current-induced magnetization switching in MgO barrier magnetic tunnel junctions with coFeB-based synthetic ferrimagnetic free layers, *IEEE Trans. Magn.* 44 (2008) 1962–1967.
- [7] P. Wiśniowski, J.M. Almeida, S. Cardoso, N.P. Barradas, P.P. Freitas, Effect of free layer thickness and shape anisotropy on the transfer curves of MgO magnetic tunnel junctions, *J. Appl. Phys.* 103 (2008) 07A910.
- [8] J.-G. Choi, D.-G. Hwang, J.-R. Rhee, S.-S. Lee, Comparison of the soft magnetic properties of permalloy and conetic thin films, *J. Magn. Magn. Mater.* 322 (2010) 2191–2194.
- [9] J.-G. Choi, D.-G. Hwang, S.-S. Lee, J.-R. Rhee, Exchange bias field and coercivity of [NiFe/NiFeCuMo/NiFe]/FeMn multilayers, *J. Korean Phys. Soc.* 62 (2013) 1954–1957.
- [10] T. Misawa, S. Mori, T. Komine, M. Fujioka, J. Nishii, H. Kaiju, Structural and magnetic properties of Ni78Fe22 thin films sandwiched between low-softening-point glasses and application in spin devices, *Appl. Surf. Sci.* 390 (2016) 666–674.
- [11] J. Son, J. Lim, J. Ko, S. Kim, S. Lee, J. Hong, A study on the sensitivity of a spin valve with conetic-based free layers, *Jpn. J. Appl. Phys.* 51 (2012) 033002.
- [12] Z.Q. Lei, G.J. Li, W.F. Egelhoff, P.T. Lai, P.W.T. Pong, Magnetic tunnel junction sensors with conetic alloy, *IEEE Trans. Magn.* 47 (2011) 714–717.
- [13] Z.Q. Lei, C.W. Leung, L. Li, G.J. Li, G. Feng, A. Castillo, P.J. Chen, P.T. Lai, P.W.T. Pong, Detection of iron-oxide magnetic nanoparticles using magnetic tunnel junction sensors with conetic alloy, *IEEE Trans. Magn.* 47 (2011) 2577–2580.
- [14] P.H. Chan, X. Li, P.W.T. Pong, Spin valves with Conetic based synthetic ferrimagnet free layer, *Vacuum* (2016), <http://dx.doi.org/10.1016/j.vacuum.2016.1009.1010>.
- [15] K. Inomata, N. Koike, T. Nozaki, S. Abe, N. Tezuka, Size-independent spin switching field using synthetic antiferromagnets, *Appl. Phys. Lett.* 82 (2003) 2667–2669.
- [16] J. Janesky, N.D. Rizzo, B.N. Engel, S. Tehrani, The switching properties of patterned synthetic ferrimagnetic structures, *Appl. Phys. Lett.* 85 (2004) 2289–2291.
- [17] S.Y. Jang, C.-Y. You, S.H. Lim, S.R. Lee, Annealing effects on the magnetic dead layer and saturation magnetization in unit structures relevant to a synthetic ferrimagnetic free structure, *J. Appl. Phys.* 109 (2011) 013901.
- [18] N. Wiese, T. Dimopoulos, M. Rührig, J. Wecker, H. Brückl, G. Reiss, Antiferromagnetically coupled CoFeB/Ru/CoFeB trilayers, *Appl. Phys. Lett.* 85 (2004) 2020–2022.
- [19] H. Y. Fredriksson, A. Alaverdyan, C. Dmitriev, D.S. Langhammer, M. Sutherland, B. Zäch, Kasemo, Hole-mask colloidal lithography, *Adv. Mater.* 19 (2007) 4297–4302.

- [20] L. Balcells, B. Martinez, O. Iglesias, J.M. García-Martín, A. Cebollada, A. García-Martín, G. Armelles, B. Sepúlveda, Y. Alaverdyan, Exchange bias in laterally oxidized Au/Co/Au nanopillars, *Appl. Phys. Lett.* 94 (2009) 062502.
- [21] P. Hanarp, M. Käll, D.S. Sutherland, Optical properties of short range ordered arrays of nanometer gold disks prepared by colloidal lithography, *J. Phys. Chem. B* 107 (2003) 5768–5772.
- [22] H.A.M. van den Berg, W. Clemens, G. Gieres, G. Rupp, M. Vieth, J. Wecker, S. Zoll, GMR angle detector with an artificial antiferromagnetic subsystem (AAF), *J. Magn. Magn. Mater.* 165 (1997) 524–528.
- [23] S.S.P. Parkin, R.F.C. Farrow, R.F. Marks, A. Cebollada, G.R. Harp, R.J. Savoy, Oscillations of interlayer exchange coupling and giant magnetoresistance in (111) oriented permalloy/Au multilayers, *Phys. Rev. Lett.* 72 (1994) 3718–3721.
- [24] J. Tang, K.-Y. Wang, W. Zhou, Magnetic properties of nanocrystalline Fe₃₀O₄ films, *J. Appl. Phys.* 89 (2001) 7690–7692.
- [25] Y.-J. Wang, C.-H. Lai, Size and shape effects on exchange field of patterned NiO/NiFe films, *J. Appl. Phys.* 89 (2001) 7537.
- [26] K. Inomata, T. Nozaki, N. Tezuka, S. Sugimoto, Magnetic switching field and giant magnetoresistance effect of multilayers with synthetic antiferromagnet free layers, *Appl. Phys. Lett.* 81 (2002) 310–312.
- [27] J. Cao, Y. Liu, Y. Ren, F. Wei, P.P. Freitas, Effect of annealing temperature on formation of superparamagnetism in CoFeB/MgO/CoFeB magnetic tunnel junctions, *Appl. Surf. Sci.* 314 (2014) 443–446.
- [28] G.V. Swamy, H. Pandey, A.K. Srivastava, M.K. Dalai, K.K. Maurya, Rashmi, R.K. Rakshit, Effect of thermal annealing on Boron diffusion, micro-structural, electrical and magnetic properties of laser ablated CoFeB thin films, *AIP Adv.* 3 (2013) 072129.
- [29] W. Bounour-Bouzamouche, S.M. Chérif, S. Farhat, Y. Roussigné, A. Tallaire, A. Gicquel, C.P. Lungu, M. Guerioune, Structural and magnetic properties of cobalt nanostructures on SiO₂/Si(1 1 1) substrates, *Appl. Surf. Sci.* 320 (2014) 858–862.
- [30] G. Herzer, Anisotropies in soft magnetic nanocrystalline alloys, *J. Magn. Magn. Mater.* 294 (2005) 99–106.
- [31] N. Tezuka, N. Koike, K. Inomata, S. Sugimoto, Single domain observation for synthetic antiferromagnetically coupled bits with low aspect ratios, *Appl. Phys. Lett.* 82 (2003) 604–606.
- [32] P. Li, G. Csaba, V.K. Sankar, X. Ju, P. Lugli, X.S. Hu, M. Niemier, W. Porod, G.H. Bernstein, Switching behavior of lithographically fabricated nanomagnets for logic applications, *J. Appl. Phys.* 111 (2012) 07B911.
- [33] N. Wiese, T. Dimopoulos, M. Rührig, J. Wecker, G. Reiss, Switching of submicron-sized, antiferromagnetically coupled CoFeB/Ru/CoFeB trilayers, *J. Appl. Phys.* 98 (2005) 103904.